



RESEARCH ARTICLE

Development of a novel body weight support system for gait rehabilitation

Lucas A. O. Rodrigues  and Rogério S. Gonçalves* 

Federal University of Uberlandia, Uberlandia, MG, Brazil

*Corresponding author. E-mail: rsgoncalves@ufu.br

Received: 18 August 2022; **Revised:** 10 October 2022; **Accepted:** 9 November 2022; **First published online:** 7 December 2022

Keywords: body weight support, gait, rehabilitation robotics, stroke, walking

Abstract

Modern rehabilitation processes for neurological patients have been widely assisted by robotic structures, with continuous research and improvements. The use of robotic assistance in rehabilitation is a consolidated technique for upper limb training sessions. However, human gait robotic rehabilitation still needs further research and development. Based on that, this paper deals with the development of a novel active body weight support (BWS) system integrated with a serious game for poststroke patients. This paper starts with a brief review of the state of the art of applied technologies for gait rehabilitation. Next, it presents the obtained mathematical model followed by multibody synthesis techniques and meta-heuristic optimization to the proposed device. The control of the structure is designed using proportional integral derivative (PID) controllers tuned with meta-heuristic optimization and associated with a suppression function to perform assist-as-needed actions. Then, the prototype is integrated with a serious game designed specifically for this application. Finally, a pilot study is conducted with the structure and healthy volunteers. The results obtained show that the mobility of the novel BWS is as expected and the proposed system potentially offers a novel tool for gait training.

1. Introduction

Stroke is defined as the loss of one or more neurological functions due to the interruption of blood flow in a certain region of the brain [1]–[8]. The rehabilitation process for stroke is currently applied through protocols developed by health professionals and potentially augmented by the use of robotic tools [9, 10].

There is evidence of the advantages promoted by the application of robotic structures in rehabilitation, such as reducing costs with active labor for training sessions and expanding the range of exercises performed [10].

The body weight-supported treadmill training emerged as one option of gait rehabilitation, where the patients were suspended by a body weight support (BWS) harness over a treadmill, while two or three therapists assisted the gait procedure, two sitting adjacent to the paretic leg to reproduce the gait movement and other therapist standing behind the patient to shift the body weight. To automatize this procedure, researchers start to develop robotic tools to replace/help the physiotherapists [10].

In ref. [12] was developed the rehabilitation robot called LOPES that is an exoskeleton attached to patients' lower limbs over a treadmill. The structure has active BWS that releases the passive weight from the lower limbs and acts only in the translation of the pelvic joint, and the pelvis rotations are constrained. In ref. [13] was explored the development of a body weight supporting while active assisting pelvic movements: vertical, lateral, and frontal translations as well as the rotation about the vertical axis.

Another example of treadmill-based structures is called robotic gait rehabilitation (RGR) [14]. It consists of a rehabilitation treadmill system designed specifically to assist in the treatment of gait in poststroke patients. The RGR robot is connected to the pelvic joint of the patient using an orthosis with two free movements in the horizontal plane and one active in the vertical direction.

The pelvic assist manipulator (PAM) is a rehabilitation structure focused on assisting treadmill exercises by actuating on the pelvic joint [15]. The movements are generated by pneumatic cylinders organized on a tripod structure that permits three active pelvis translations and two rotations with the pelvic tilt not controlled.

One commercial rehabilitation device that applies BWS and a treadmill is the Lokomat (Jezernik *et al.*, 2004). This robotic orthosis features two serial structures that actuate directly on the lower limbs during rehabilitation training sessions. Lokomat has an optional module that permits the lateral translation and transverse rotation of the pelvis [16].

The body weight support system (BWSS) can aid in gait rehabilitation providing weight relief that reduces the muscle's demand and can make it easier to coordinate limb motion. The use of BWSS permits patients with limited strength training the walking [17]. Studies realized indicated that BWSS to gait practice can improve walking ability in people with stroke, Parkinson's, or incomplete spinal cord injury [17].

Despite the advances in the application of BWSS in gait rehabilitation, the benefits have been inconclusive. It appears that robotic structures for rehabilitation on treadmills with passive weight support influence the balance and movements of the pelvis and thorax during gait [18, 19]. The design of the BWSS user alone or together with gait training robots, usually, is a static device that does not adapt to changes in trunk height. Some BWSS have passive or controllable vertical movements but limited pelvis movements.

In this paper, the development of a novel structure for the rehabilitation of human gait is carried out, aimed at the treatment of victims of stroke, cerebral palsy, and other pathologies that cause problems in the rhythmic gait, aiming to promote functional gains to patients, increasing the motor capacity of the patients injured lower limb. It is noteworthy that this paper brings innovation to the rehabilitation of human gait assisted by robotic structures by proposing a parallel structure of five degrees of freedom based on a family of mechanisms with low coupling between joint coordinates. Through the use of this unique design for the rehabilitation of human gait, the aim is to obtain a structure capable of withstanding the passive weight of patients and promoting controlled actions without the need for high-power actuators and without compromising the workspace with singularities.

This work proposes the use of an active BWS acting on the relevant degrees of freedom of the pelvis for the rehabilitation of human gait capable of performing the three translations, and rotations under the frontal and transverse planes, restricting only the sagittal plane.

This paper is structured as follows: Section 2 explains the importance of the pelvic joint, Section 3 provides the mathematical model of the proposed novel BWSS, followed by the implementation of the mechanical structure, Section 4, and the control system design, Section 5. The serious game developed is presented in Section 6. The experimental tests and results are analyzed and discussed in Section 7. Finally, the conclusions and recommendations are drawn in Section 8.

2. Pelvic joint movements

The sacroiliac joint, also known as the pelvic joint, is the connection between the base of the cervical spine (sacral bone) and the articular surfaces of the ilium of the pelvis. It is a joint of low mobility and high stability and plays a key role in balance. In this way, the physiological function of this joint is more connected to stability than to excess mobility. Although the range of your movements is limited, these are important to ensure the stability of the body when associated with hip and low back movements. This mobility can even functionally help patients with gait irregularities [20]. The sacroiliac joint has three degrees of freedom of rotation with the following amplitudes: 25° of rotation in the transverse plane, 5° of rotation in the sagittal plane, and 2° of rotation in the frontal plane [21].

This paper describes the novel BWSS device for gait rehabilitation through pelvis facilitation movements. Five degrees of freedom are actuated: vertical, transverse, and frontal translation as well as the rotation about the frontal and transverse planes, Fig. 1.

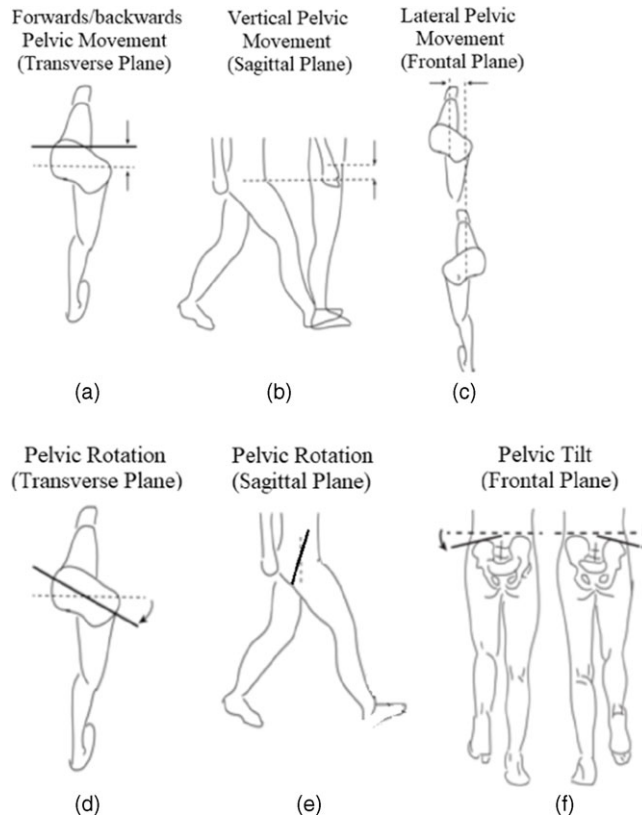


Figure 1. Pelvis movements associated with the gait.

Pelvic facilitation is a method used by physiotherapists together with treadmill-based therapies that include pelvis movements. Some robotic trainers focus on the leg and feet, and evidence from the literature indicates that a pelvis-based robot could have a large impact on the gait [22]. The movement of the pelvis can impart swing energy to the leg even when hip and knee muscles are weak, and a pilot study found that patients who were being rehabilitated through pelvis actuation showed more brain activity compared to the patients rehabilitated by moving the legs through gait [23].

The pelvis motions involve the translation vertical, lateral and frontal movements, and transverse, coronal and sagittal rotations, as shown in Fig. 1.

The pelvis transverse translation, as shown in Fig. 1(a), is relative to average forward/backward displacement. The transverse displacement could improve gait symmetry and gait speed.

The pelvic vertical translation degree of freedom, as shown in Fig. 1(b), is related directly to the BWS forces. The literature showed that stroke treadmill training using BWS is more effective than with no BWS [24]. The BWS supports part of the patient's weight and reduces the amount of muscle function required to walk facilitating the rehabilitation process early. The possibility of vertical BWS can help the patient transfer energy between the gravitational potential to kinetic forms making the gait process more energy efficient.

The lateral pelvic movement, as shown in Fig. 1(c), is necessary to weight shift towards the stance leg that allows the swing leg to be lifted. The stroke can cause asymmetric deficiencies, and the patients can have difficulty balancing on their paretic limb which is used in conventional physiotherapy [23]. The pelvis transverse rotation, as shown in Fig. 1(d), permits the hips to move frontally relative to each other. Combining transverse displacement and transverse rotation could prevent knee hyperextension in stroke patients [23].

The pelvis sagittal rotation, as shown in Fig. 1(e), on the axis of rotation, that connects the hips is not used in the gait process directly [13, 23] and is not considered an active degree to be controlled in this paper.

The pelvis frontal rotation, as shown in Fig. 1(f), occurs when one hip rises relative to the other. Stroke patients can produce abnormal frontal rotations while walking to increase ground clearance for the paretic leg swing side. The physiotherapists compensate for this problem by pushing down on the affected side of the hip during the swing which involves uncomfortable postures for the health professional.

The importance of freedom for the movement of the pelvis is further evidenced when analyzing the so-called pelvic step, which consists of the rotation movement of the pelvis in the transverse plane, which increases the step length during human gait, reducing the vertical movements of the pelvis and center of mass of the body [23]. Although it has been shown that transverse rotation of the pelvis may be out of phase with hip movement during gait at low speeds and small steps, this movement may help patients with low mobility for hip flexion movements to increase stride length, which can contribute to increasing their mobility [23]. There is also evidence that restriction of pelvis movement can also significantly interfere with stride width and rotations in the frontal and sagittal planes of the body during gait and should be avoided for more efficient training [24].

3. Mathematical modeling of the novel active BWS

The proposed novel active BWSS consists of a parallel robotic structure with five degrees of freedom, three degrees related to three-dimensional spatial translation, and two degrees of rotation. The main therapeutic objective of this support is to promote assisted training of the pelvic joint during the gait training session. In this way, the structure aims to promote more efficient training capable of facilitating improvements in patients' balance.

3.1. Inverse geometric model

The design of the structure was carried out to minimize the coupling of the joint coordinates of the structure through the application of an architecture based on the “multipteron” family [25, 26], keeping only the sagittal movement of the pelvis mechanically restricted due to its low influence on the rehabilitation process of human gait [13, 23]. For this, we propose the application of a structure defined as 4-PRRU + PRRS as a form of “pentapteron,” as shown in Fig. 2, where P is an actuated prismatic joint, R represents a rotational joint, U is a universal joint, and S represents a spherical joint. Point P of the mobile platform is the point where a seat for the patient will be installed.

In Fig. 2, translational and rotational joints have been grouped into cylindrical joints $q_i, i = 1$ to 5 , to facilitate representation in the scheme. However, translation and rotation joints were used during the construction of the prototype described in Section 4. The universal joints are represented by cross-cylinders, and the spherical joint as a dashed circumference placed behind the mobile platform, Fig. 2.

For the modeling of this system, equipollent coordinates [27] were used for the references illustrated in Fig. 2(a) so that each joint coordinate q_i is in one of the directions of the unit vectors of the frame of reference. Therefore, for each leg i , the vector u_i that connects the active joint of this leg to one of the points on the mobile platform that belongs to a plane perpendicular to the unit vector of the actuator direction is highlighted. Based on these facts, we proceed with the modeling of this structure, analyzing each leg i individually and systematizing the equations obtained in a matrix relating to the joint and operational coordinates.

To analyze the position of point A of the mobile platform from a leg i in relation to the inertial reference can be equated with the position in relation to the references of the leg in question. For the case of leg 1, this relationship is illustrated in Fig. 3 and formalized in (1).

$${}^0\mathbf{r}_p + \mathbf{r}_A = {}^0\mathbf{r}_1 + q_1\mathbf{i}_1 + \mathbf{u}_1 \quad (1)$$

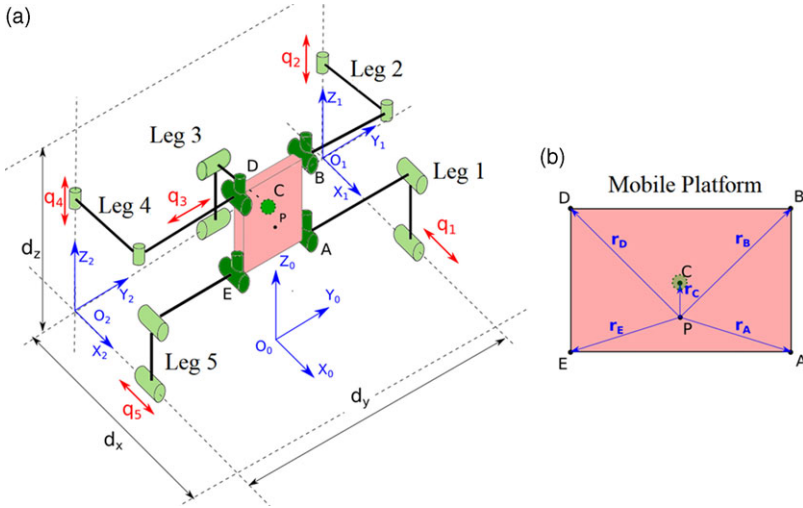


Figure 2. (a) Schematic drawing for the structure of the active support of the pelvis, based on the “pentapteron” (4-PRRU + PRRS); and (b) position of the point of interest P in relation to the vertices of the mobile platform.

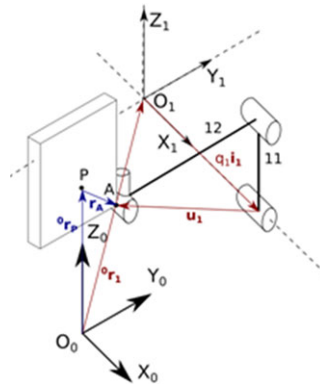


Figure 3. Analysis of the position of point A in relation to the inertial frame and leg 1.

where ${}^0\mathbf{r}_p$ is the position of point P with respect to $X_0Y_0Z_0$, \mathbf{r}_A is the relative position of point A with respect to point P, and \mathbf{i}_1 is the unit vector of the X direction of reference frame $X_1Y_1Z_1$. The vector \mathbf{u}_1 belongs to a plane parallel to the plane Y_1Z_1 , therefore perpendicular to the unit vector \mathbf{i}_1 , and that $\mathbf{i}_1 = \mathbf{i}_0$ due to the fact of adopting references with equipollent coordinates. Therefore, when performing a dot product on both sides of (1) by \mathbf{i}_0 :

$$q_1 = ({}^0\mathbf{r}_p + \mathbf{r}_A - {}^0\mathbf{r}_1) \cdot \mathbf{i}_0 = \left(\left\{ \begin{matrix} 0 & r_{px} & r_{py} & r_{pz} \end{matrix} \right\} + \{r_{Ax} \ r_{Ay} \ r_{Az}\} - \left\{ -\frac{dx}{2} \ \frac{dy}{2} \ 0 \right\} \right) \cdot 100 \Rightarrow q_1 = {}^0r_{px} + \frac{dx}{2} + r_A \cos \phi \tag{2}$$

where ϕ corresponds to the angle between the vectors \mathbf{r}_A and \mathbf{i}_0 , as illustrated in Fig. 4, which is also defined as the orientation of the mobile platform in terms of its rotation around the Z_0 axis.

The analogous procedure is made to legs 2 to 5 to obtain the following equations:

$$q_2 = ({}^0\mathbf{r}_p + \mathbf{r}_B - {}^0\mathbf{r}_1) \cdot \mathbf{k}_0\mathbf{q}_2 = {}^0r_{pz} + r_B \cos \theta \tag{3}$$

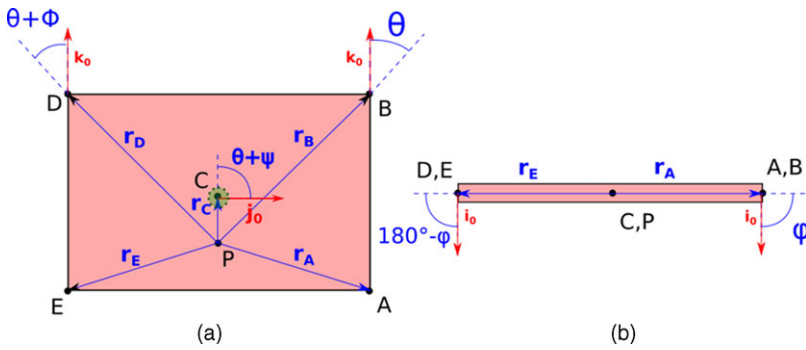


Figure 4. Angles between the unit vectors and the position vectors of the ends in relation to point P: (a) angles of rotation around X_0 ; and (b) rotation around Z_0 .

where angle θ corresponds to the angle between the unit vector k_0 and the vector r_B , as illustrated in Fig. 4.

$$q_3 = {}^0r_{py} + r_C \cos(\theta + \psi) + \frac{dy}{2} \tag{4}$$

where angle $\phi + \psi$ represents the orientation around the X_0 axis of the mobile platform, as shown in Fig. 4.

$$q_4 = {}^0r_{pz} + r_D \cos(\theta + \phi) \tag{5}$$

where angle $\theta + \phi$ is the angular difference between vector r_D and unit vector k_0 , as defined in Fig. 4.

$$q_5 = {}^0r_{px} - r_E \cos(\phi) + \frac{dx}{2} \tag{6}$$

Equations (2) to (6) present the relations of the operational coordinates 0r_p , θ , and ϕ with the joint coordinates q_1, q_2, q_3, q_4 , and q_5 . Through these, it is possible to find the Jacobian matrix of the structure, which is used to determine the possible singular positions.

3.2. Singularity analysis

First, it is necessary calculate the time derivative of (2) to (6). Their respective time derivatives are presented in (7a) to (7e) and the matrix form, $[J_q]\{\dot{q}\} = [J_x]\{\dot{x}\}$, that groups these equations is presented in (7f):

$$\dot{q}_1 = {}^0\dot{r}_{px} - r_A \sin(\phi)\dot{\phi} \tag{7a}$$

$$\dot{q}_2 = {}^0\dot{r}_{pz} - r_B \sin(\theta)\dot{\theta} \tag{7b}$$

$$\dot{q}_3 = {}^0\dot{r}_{py} - r_C \sin(\theta + \psi)\dot{\psi} \tag{7c}$$

$$\dot{q}_4 = {}^0\dot{r}_{pz} - r_D \sin(\theta + \phi)\dot{\theta} \tag{7d}$$

$$\dot{q}_5 = {}^0\dot{r}_{px} + r_E \sin(\phi)\dot{\phi} \tag{7e}$$

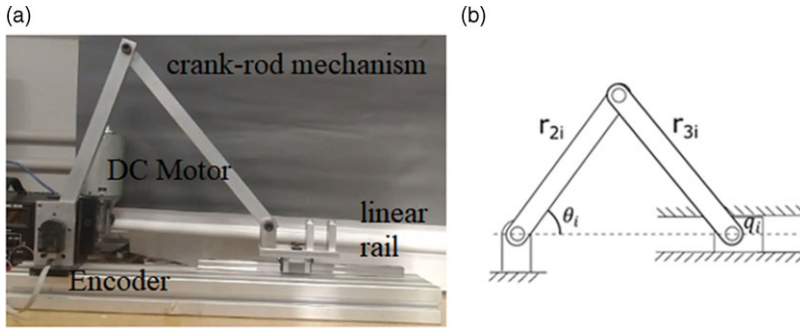


Figure 5. (a) Prototype of the motor module and (b) schematic drawing of the mechanism.

$$[J_q] \{\dot{q}\} = [J_x] \{\dot{x}\} \Rightarrow \begin{pmatrix} \dot{q}_1 \\ \dot{q}_2 \\ \dot{q}_3 \\ \dot{q}_4 \\ \dot{q}_5 \end{pmatrix} = \begin{bmatrix} 1 & 0 & 0 & 0 & -r_A \sin(\varphi) \\ 0 & 0 & 1 & -r_B \sin(\theta) & 0 \\ 0 & 1 & 0 & -r_C \sin(\theta + \psi) & 0 \\ 0 & 0 & 1 & -r_D \sin(\theta + \phi) & 0 \\ 1 & 0 & 0 & 0 & r_E \sin(\varphi) \end{bmatrix} \begin{pmatrix} {}^0\dot{r}_{P_x} \\ {}^0\dot{r}_{P_y} \\ {}^0\dot{r}_{P_z} \\ \dot{\theta} \\ \dot{\varphi} \end{pmatrix} \quad (7f)$$

In this way, it is possible to notice that $[J_q] = [I]$, which means that the singular positions will exist only for the case where $\det([J_x]) = 0$. Therefore, these cases can be expressed according to (8):

$$\begin{aligned} \det([J_x]) &= r_A r_D \sin(\phi + \theta) \sin(\varphi) - r_B r_E \sin(\theta) \sin(\varphi) - \\ &\quad - r_A r_B \sin(\theta) \sin(\varphi) + r_D r_E \sin(\phi + \theta) \sin(\varphi) = 0 \\ &\Rightarrow r_D \sin(\phi + \theta) = r_B \sin(\theta) \end{aligned} \quad (8)$$

Therefore, whenever (8) is true, the system will be in a position of singularity and will be subject to loss of control and/or problem of mobility in this position. Based on this information, to design this structure it is necessary to guarantee that the selected dimensions of r_B , r_D , and ϕ do not allow the occurrence of (8) at no point in the workspace at θ . It is also possible to notice that the translational degrees of freedom of this structure are limited only by the respective limits of the workspace, since these do not present terms in the Jacobian matrix $[J_x]$.

To reduce the cost of high-speed linear actuators, an actuator model was proposed, based on 24-V DC motors coupled to rotary encoders, and the angular movement of these motors was transformed into linear displacement through a 3-bar crank-rod mechanism type. The scheme designed for this system is represented in Fig. 5, and the relationship between q_i and θ_i is described in (9).

$$q_i = r_{2i} \cos \theta_i + \sqrt{r_{3i}^2 - r_{2i}^2 \sin^2 \theta_i} \quad (9)$$

3.3. Dynamic model and simulation optimization

To define the dimensions of the mechanical elements and actuators, a computational model considering geometric and dynamic characteristics was developed. The patient’s mass was considered as punctual dynamic loading generated by it on the linear guides q_i and transmitted to the DC motors M_i through the connecting crank-rod mechanism. The approach is valid due to the low speeds and accelerations present in the kinematics of human gait rehabilitation [28]. Therefore, the mass and inertia of the bars

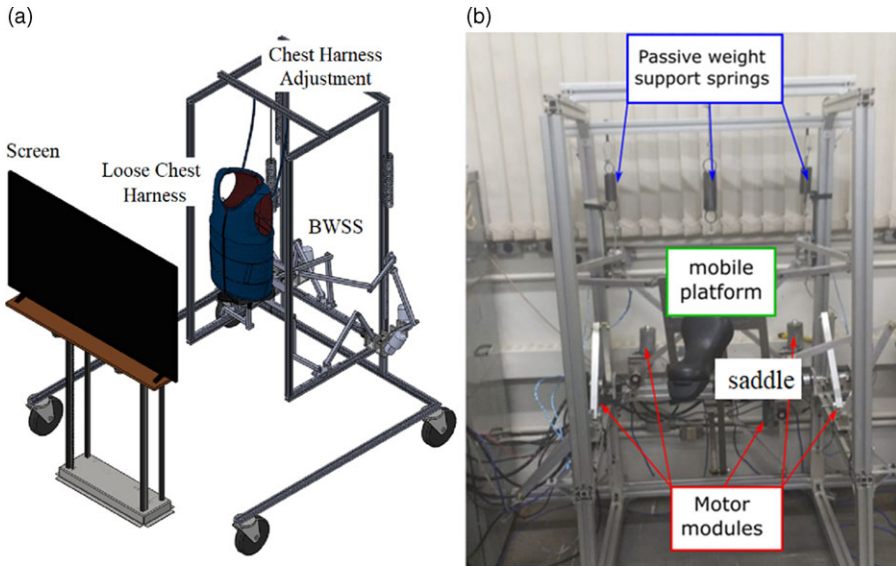


Figure 6. (a) CAD version and (b) the built prototype.

and other mechanical elements present in this module can be disregarded without prejudice to the system specifications. A critical mass $M_p = 150 \text{ Kg}$ was considered.

The movement requirements were established according to the human gait with a focus on the sacroiliac joint, as shown in Table V.

For the calculation of the dynamic model, it was considered: bars that connect the module’s mobile platform to the linear guides must withstand the maximum static load, specified as the critical mass of the system; linear guides must traverse the specified workspace within the critical cycle time ($t_c = 0.4 \text{ s}$); bars that connect the linear guides to the DC motors must punctually support the maximum dynamic load, disregarding the effect of inertia to simplify the model; actuators 2 and 4 will be implemented together with a passive spring system to relieve the patient’s static load, as shown in Fig. 6, allowing actuators to focus only on dynamic efforts; and an additional spring has been connected to the mobile platform, as shown in Fig. 6, without prejudice the defined workspace, to improve the passive support of the structure and relieve the static load of the other actuators.

Therefore, from the proposed directives, it is defined that the linear guides must be able to start their respective trajectories from the beginning of the course with zero initial velocity and finish the movement in the final position again with zero velocity. The dynamic equation that defines the greatest effort F_i applied under each actuator q_i can be defined as:

$$F_i = f_{r_i} M_p \frac{d_i}{t_c^2} \quad i = 1, 2, 4, 5 \Rightarrow f_{r_i} = 0.5 \quad i = 3 \Rightarrow f_{r_i} = 1 \quad (10)$$

where d_i corresponds to the working space specified for each linear guide rail, t_c is the time to complete the gait cycle considered as 0.4 s, and the parameter f_{r_i} corresponds to a correction factor applied in the equation to consider the weight distribution between actuators 1 and 5, and actuators 2 and 4. The actuator 3 acts alone in the j_0 direction, which means that it does not need correction, and therefore $f_{r_3} = 1$. The model also considers the minimum requirements for electrical power and angular speed of the specified DC motors to allow the correct movement of the connecting crank-rod mechanism. A free body diagram was constructed showing the considered efforts, as shown in Fig. 7. In this diagram, T_i represents the input angular momentum of the motor M_i , and F_i is the force applied on q_i .

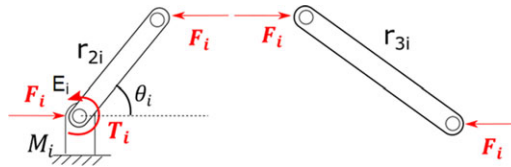


Figure 7. Free body diagram of the connecting crank-rod mechanism of the actuators.

Applying the equilibrium moment conditions to the free body diagram in Fig. 7, with respect to the point E_i , the moment T_i can be written as:

$$T_i = F_i r_{2i} \sin \theta_i \tag{11}$$

differentiating (9) in time and isolating $\dot{\theta}_i$ is obtained:

$$\dot{\theta}_i = \frac{\dot{q}_i}{-r_{2i} \sin \theta_i - \frac{r_{2i}^2 \sin \theta_i \cos \theta_i}{\sqrt{r_{3i}^2 - r_{2i}^2 \sin^2 \theta_i}}} \tag{12}$$

Therefore, to obtain the expression for the minimum power required for each electric motor is applied (13):

$$P_i [W] = \frac{\theta_i \tau_i}{9.55} \tag{13}$$

To calculus the tension applied to the cross sections of each bar, was used as a criterion for the comparison σ_{ij} of the stress calculated in each cross section through the theory of strength of materials [29], according to (14), where F_j are the efforts applied to the element, r_{ij} is the analyzed bar, and I_{ij} is the moment of inertia of the bar:

$$\sigma_{ij} = \frac{F_j r_{ij}}{4I_{ij}} \tag{14}$$

To obtain the optimal dimensions of the bars that will compose the mechanism, the tension calculated according to (14) is compared with the yield strength of the selected material defined as aluminum ($\sigma_{max} = 180$ MPa). To facilitate the bar specification process and reduce manufacturing costs, all bars in the system were considered as rectangular tubes with cross sections compatible with the materials available. The factor of safety equal two was used. All the requirements were combined in a computational model developed in MATLAB® together with a differential evolution algorithm forming an interactive simulation optimization system. The simulation optimization parameters are number of replications = 10, population size = 50, maximum iterations = 200, crossover rate = 0.8, and mutation probability = 0.005.

The results obtained through this process are shown in Table I. The bars r_{2i} and r_{3i} are the ones that make up the connecting crank-rod mechanism of each actuator i , being all similar to each other, as shown in Fig. 5. The bars r_{4i} and r_{5i} represent the connection bars between the linear guide rail and the mobile platform for each leg i , as shown in Fig. 1.

The simulation also determined the necessary characteristics for the DC motors, as shown in Table II, as described in (12) and (13).

4. Implementation of BWS

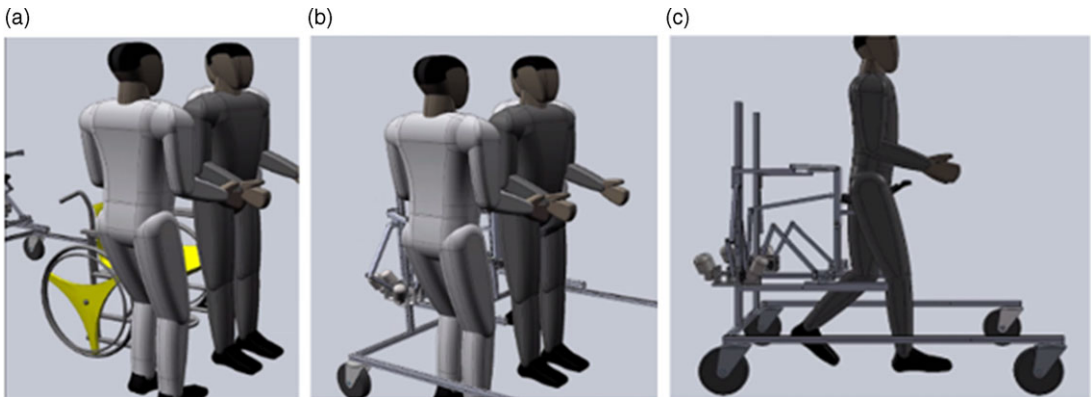
This section presents the design and implementation of the active BWSS for gait rehabilitation. The manufacture prototype is shown in Fig. 6(b). The novel proposed device is designed to impose minimum constraints on the user, with intrinsically minimizes the donning and doffing time, as shown in Fig. 8. The proposed device can be used for overground rehabilitation in patients that can walk alone, as shown in Fig. 8(c), or together with a treadmill, or other exoskeletons that can be coupled with the legs.

Table I. Optimal dimensions calculated for each module bar.

Link	Length (mm)	Cross section (mm)	Thickness (mm)
r_{2i}	250	25.4	5
r_{3i}	300	25.4	5
r_{4i}	300	25.4	5
r_{5i}	300	25.4	5

Table II. Specifications for the module's DC motors.

Motor	Power required (W)	Required angular velocity (RPM)
M_2	35	20
M_3	20	15
M_4	20	10
M_5	20	15
M_5	35	20

**Figure 8.** The sequence of the image shows the patient donning process. (a) Removing the patient from the wheelchair; (b) donning the patient to the device; and (c) overground rehabilitation exercises.

The proposed device is used in the pilot study with a treadmill (Movement R4, 1250 × 440 mm, speed 1 to 14km/h), utilized to forward propulsion and simulate the gait together with the serious game developed. The use of the treadmill is justified in the function of the availability of this device in rehabilitation clinics [30].

The interaction between the structure and the user is made by a saddle, as shown in Figs. 5 and 9(a). This seat shape was chosen based on studies carried out in refs. [28]–[31] that showed the best comfortable shape to support the patient weight. The saddle is rigidly fixed on the mobile platform, as shown in Fig. 9(a). If necessary for the safety of the patient one conventional overhead BWSS can be used to “catch” the subject, thus preventing falls. Figure 9(a) is shown the connected joints to the mobile platform, universal joints in points A, B, D, and E, and spherical joint (point C), Fig. 2.

Figure 9(b) shows the constructive elements of the motor module: crank-rod mechanism; DC motor; incremental encoder; and linear rail and end of course switch. Incremental encoders are used, and the initial position is set using the end of course switches. The leg is composed of the links, revolute joints, and the coupling joint in the mobile platform, Fig. 9(b).

Table III presents the actuation components specifications used in the built prototype. These are low-cost components available in the laboratory.

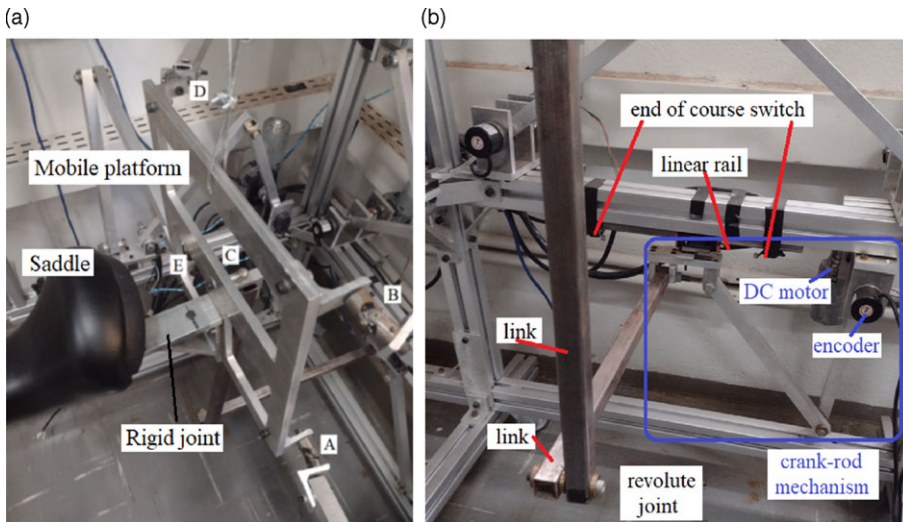


Figure 9. (a) Connect joints to the mobile platform and (b) details of leg 3.

5. Control design

The control scheme of each actuator is represented in Fig. 10.

For each module, a controller divided into two parts was specified: a proportional integral derivative (PID)-type position controller, tuned using an optimization system based on a differential evolution algorithm, and an “assist-as-needed” (AAN) to dynamically suppress PID action, applying it only when needed by the patient. The AAN works like a check function that says whether the error is inside the dead zone. For each encoder, an interrupt-enabled, general-purpose pin was used. As described by the official microcontroller documentation, the ideal scenario for deterministic control should have two interrupt pins for each channel of each encoder. Due to the unavailability of sufficient pins, the control used a nondeterministic configuration, where the pulse count is subject to pulse losses. The equation used was as follows:

$$u[kT] = K_p e[kT] + K_I \int_0^T e[kT] dT + K_D \frac{d}{dT} e[kT] \tag{15}$$

where K_p is a proportional constant, K_I is an integral constant, K_D is the derivative constant, $u[kT]$ represents the discrete output signal of the PID controller as a function of sampling time T , and $e[kT]$ is the system error calculated as a function of the system reference. Using a controller, it is possible to make the actuator meet design requirements, such as maximum position error ϵ , settling time t_s , and maximum overshoot [32]. However, due to the lack of determinism implied by the limitations of the microcontroller used, the control law of (15) is subject to variations in the sampling period T . Thus, the use of a differential evolution optimizer was necessary to guarantee stable parameters that compensated this problem. The control of the actuators was designed according to the following criteria: settling time t_s less than 0.2 s, overshoot close to zero, and zero stationary error.

Therefore, to estimate the parameters K_p , K_I , and K_D , it used a meta-heuristic optimization system based on a differential evolution algorithm [33]. To use this system, several tests were performed automatically in the system, analyzing the system response to a known fixed input and collecting the corresponding response telemetry of each execution. The individuals used in this algorithm had three genes, where each one represents one of the controller constants K_p , K_I , and K_D .

The controller optimization process was performed for each controller separately, following the following parameters: population size (number of individuals): 30; the maximum number of iterations (maximum generations): 30; mutation rate: 0.5%; binomial random crossing probability: 80%; side

Table III. Actuation components specification.

Component	Specification	Quantity
Motor DC 24V Bosch F006WM0310	46W, 51 RPM, 63:1	5
Rotary Encoder HEDS 5540	500 pulses	1
Rotary Encoder NPN LPD3806-600BM-G5-24C	600 pulses	4
Linear guide with ball screw slide	300 mm	5
End of course switch	–	10
Microcontroller Arduino Mega 2560	–	1
DC motor drive shield VNH2SP30	16V 30A	4
Variable DC source 0 to 30V	–	1

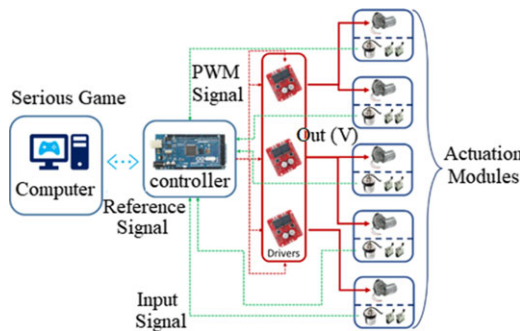


Figure 10. Control scheme applied to the active weight support prototype.

limits of variables: K_p from 0.1 to 4.0; K_I from 0.0 to 1.0; and K_D from 0.0 to 2.0. After optimizing, the obtained results are presented in Table IV.

To implement the AAN behavior, an additional portion was applied to each controller according to the block diagram as shown in Fig. 11, capable of generating a zone where its action is suppressed, called “dead zone” [34]. This zone consists of a range of system error values and is empirically defined as a function of the characteristics of the controlled system, which, in the case of assisted rehabilitation, represents the region where the patient will exercise motor action without the need for a controller.

On the other hand, whenever the system error exceeds the dead zone, the controller’s control action will be applied again, representing the absence of the patient’s motor action and implying the need for intervention by the structure. The dead zone implementation is done through a combination of the controller action with a hyperbolic tangent function. The choice of this function guarantees a smooth transition between the dead zone and the controller’s action regions and weights the controller’s action to avoid sudden movements during the training session. To avoid system instabilities when the error is inside the dead zone, part of the system reference is passed directly to the control action, known as feedforward. Thus, the control action of the system is described in (16):

$$u_a[kT] = K_p \tanh(\gamma u[kT]^3) + K_f \tanh([kT]^3) \tag{16}$$

where K_p represents the proportional gain of the system, $u[kT]$ is the control signal of the PID controller, γ is the constant used to delimit the dead zone, K_f is the gain associated with the feedforward portion of the system, and $r[kT]$ is the system position reference.

6. Space Walker serious game

The serious game, named Space Walker, is designed to match the required characteristics to react to the movements in the training sessions with the proposed BWSS and also intends being functional and

Table IV. Actuation components specification.

Motor	K_P	K_I	K_D
1	2.78460	0.00000	0.12855
2	1.68340	0.00000	0.06866
3	3.07820	0.00000	0.08302
4	1.45780	0.38957	0.09438
5	4.00000	0.00000	0.10293

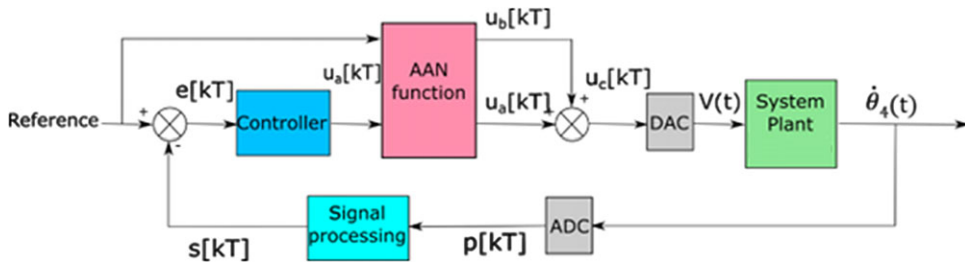


Figure 11. Control loop applied to actuators, including a PID controller and an AAN function.



Figure 12. (a) Screenshot of Space Walker showing the main character walking in the infinite platform and (b) bonus cube (green) in the scene.

fun. Since this rehabilitation structure deals with tridimensional movements, the game was designed using the software Unity 3D with the theme of the endless runner (in which the character moves forward automatically and the user controls lateral movements moving laterally over the treadmill). The main character of the game is a humanoid robot that walks on an infinite platform with three main lanes, one to the left, one in the middle, and one to the right. During the walk, the player must avoid collisions with obstacles and collect bonus items. A screenshot of the main game interface is shown in Fig. 12(a).

The character humanoid robot is programmed to walk in a straight line and change lanes. Its position is hardwired to the encoder readings of q_3 in the proposed active BWSS. Thus, the humanoid robot should follow the same position as the user, creating an immersive sensation with the serious game.

The game starts with an initial screen where the health professional enters the desired duration for the training session and adjusts the translation of the mobile platform to the neutral position of the patient. After the position is adjusted, the treadmill is turned on and the game starts. The structure sends periodical data containing information about the patient’s position that controls which lane the main character should walk in. The periodical signals of the microcontroller are sent through the USB

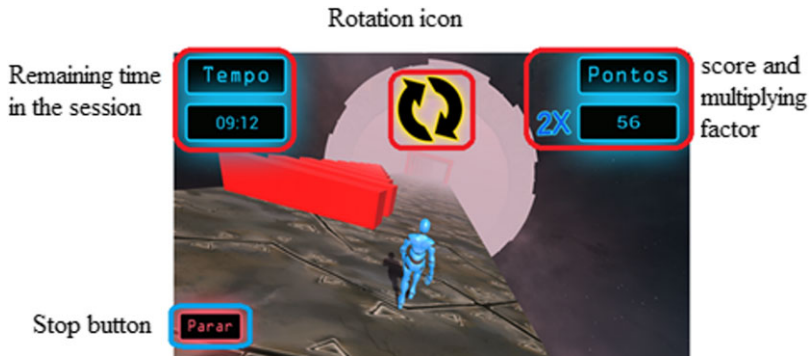


Figure 13. Interface diagram of the platform rotation.

connection every 500 milliseconds, with the position of the patient along Y_0 measured in the rotary encoder of q_3 . This encoder has 500 pulses per cycle, resulting in a workspace of around 200 pulses for the motor modules.

Therefore, three zones are defined to represent the lanes of the game based on the encoder readings: up to 60 pulses, the microcontroller sends a message indicating the left lane; from 61 to 120, it indicates the central lane; and above 120 pulses, the right lane. If the player finds difficulties avoiding collisions with the obstacles, the game will send a command to activate the assistance in q_3 to assist the patient to move the character to the correct lane. To do this, a script counts the collisions per minute of the player, and if the value is greater or equal to 4, this command is sent to the structure. Once the collisions per minute are reduced, the assistance is turned off.

The score in the developed game is directly proportional to the time of the session, where the player continuously earns points as long as the training session is active. The game also has extra points that can be obtained by collecting bonus cubes, as shown in Fig. 12(b), or multiplying the base score when the mobile platform of the active BWSS is rotated together to rotate the scenario, as shown in Fig. 13.

The rotations of the game platform are randomly activated in an arbitrary interval between 60 and 100 s. The same command sent to the proposed BWSS is sent to the camera, creating a sensation that the same action happening in the virtual environment is being replicated in the reality. During the platform rotations, an animated icon also pops up in the game interface, as shown in Fig. 13.

The bonus cubes are small floating green objects that spawn eventually with the tiles, as shown in Fig. 12(b). These cubes appear in one defined lane of the platform and are not always easily reachable. More information about the serious game developed can be found in ref. [35].

7. Experimental tests

Experimental tests were carried out to: verification of the movements and validation of the angular amplitude of the mobile platform; verification of control requirements; validation of module resolution; and comparison of CAD/CAE model and prototype response.

7.1. Movements of the novel active BWS

The proposed movements of the novel active BWS are presented in Fig. 14. The measurements of the mobile platform were performed using a digital inclinometer (resolution of 0.1°) to define the actual workspace of the structure and compare it with that specified in the mathematical model. In this experiment, 10 repetitions were also performed for each measured angular degree of freedom. In the case of linear degrees of freedom, the nominal measures of the linear guides applied to the structure were used as the workspace. The results are presented in Table V.

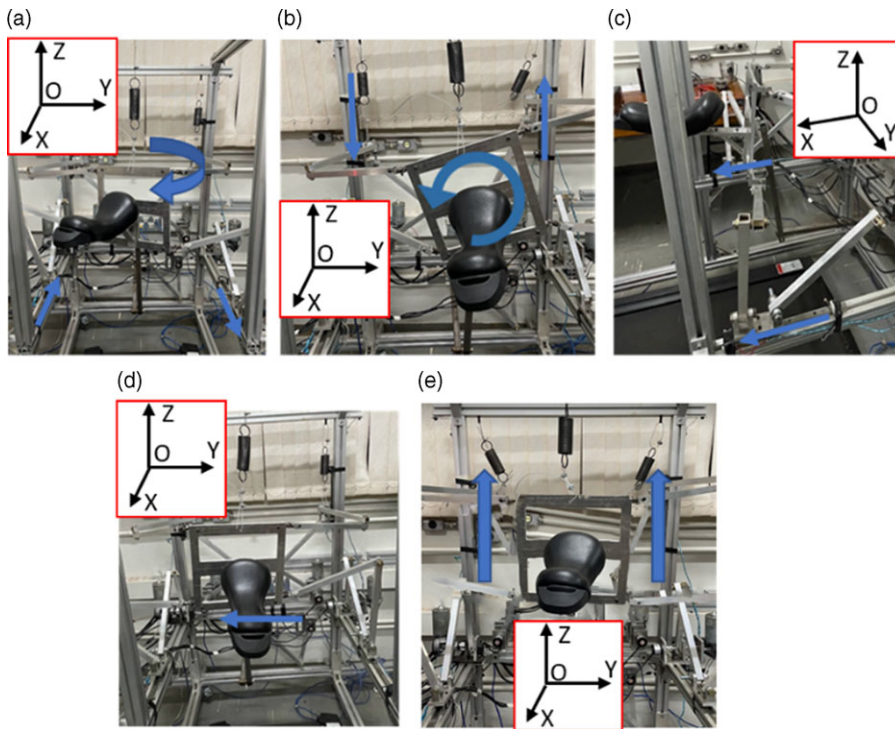


Figure 14. Movement tests of the mobile platform of the novel BWSS prototype. (a) Rotation in the transverse plane (about the OZ axis); (b) rotation in the frontal plane (around the OX axis); (c) translation on the OX axis; (d) translation on the OY axis; and (e) translation on the OZ axis.

From Table V, it is possible to notice that the workspace obtained in the prototype meets the proposed specifications considering the mobility of the pelvic joint. It is also noted that the selected design also allows angular amplitudes above the minimum, which will allow the structure to be used to perform controlled movements for balance training.

A comparison was made with the points obtained for one of the motors of the structure about the same movement performed by the CAD/CAE model developed [36]. In this experiment, a simulation of the mechanical system was performed moving 150 mm in 0.4 s, and the points obtained were saved. Afterward, the same movement was performed 10 times on one of the structure's motors, and the telemetry was collected. The comparison between the simulated and experimental results is represented in Fig. 15.

7.2. Verification of control requirements

The test carried out sought to validate whether the use of the differential evolution algorithm was able to obtain the constants K_p , K_I , and K_D capable of meeting the requirements proposed in Section 5.

The experiment carried out consisted of saving the data recorded in the input, output, and time Arduino when performing a displacement of 200 pulses and analyzing them using open Data Science libraries in Python and Jupyter Notebooks. The results obtained are visually represented through histograms as shown in Fig. 16.

Through the visual analysis of the collected data, it was possible to notice that the specified accommodation time was consistently met, ensuring that the system presents an adequate response. Although the stationary error has been specified as null and the mechanical characteristics of the system guarantee

Table V. The amplitude of the mobile platform measured experimentally.

Degree of freedom	The amplitude of the pelvis	The amplitude of the structure	Experimental
X-Translation	–	$\pm 100\text{ mm}$	$\pm 200\text{ mm}$
Y-Translation	–	$\pm 200\text{ mm}$	$\pm 200\text{ mm}$
Z-Translation	–	$\pm 150\text{ mm}$	$\pm 200\text{ mm}$
X-Rotation	$\pm 5^\circ$	$\pm 5^\circ$	$-33.4^\circ + 35.4^\circ$
Z-Rotation	$\pm 25^\circ$	$\pm 25^\circ$	$-36.5^\circ + 32.6^\circ$

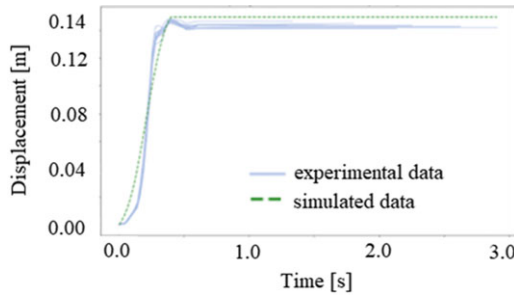


Figure 15. Comparison between the experimental data measured in one of the prototype actuators and the data simulated in CAD.

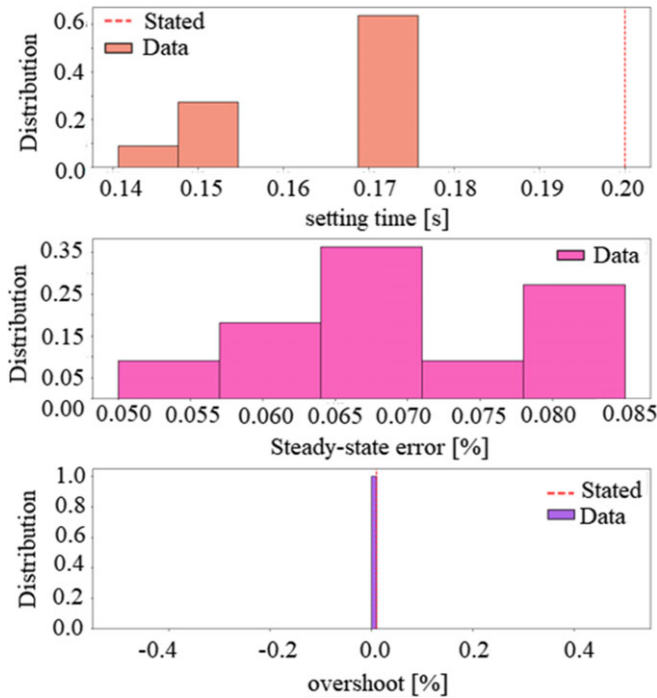


Figure 16. Histogram representing the distribution of the results obtained in the 11 repetitions of the control requirements validation experiment. From top to bottom, Settling Time Analysis Results, Percent Stationary Error, and Overshoot.

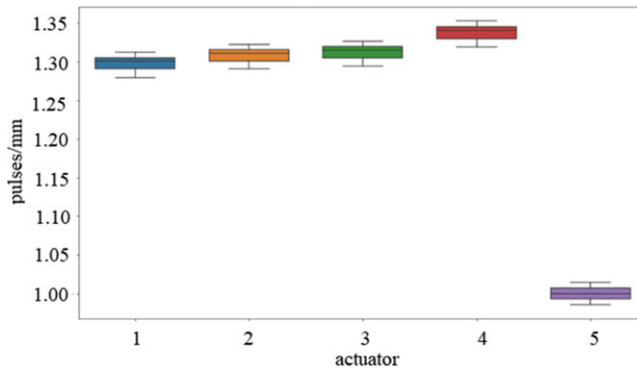


Figure 17. Boxplot graph of the resolution calculated for each actuator, in pulses/mm.

a transfer function with Type Number 1, the error cannot be eliminated. This error will need to be investigated in detail in future works and may be linked to the limitations of the microcontroller. However, considering the constructive aspects of the structure, the stationary error of the structure can still be considered tolerable and not cause significant problems in the movement of the platform, guaranteeing the functionality of the equipment. In addition, the system did not show overshoot in any of the samples. This also ensures that frame-specified movements will not expose patients to an excessive range of motion and will prevent vibrations when reaching the desired position.

Another experiment carried out sought to validate the relationship between the number of pulses measured in the encoders. To carry out this experiment, a displacement of 200 pulses was applied to each of the motors with 10 repetitions, and the displacement of the linear cursor was measured with the aid of a precision ruler (resolution of 0.5 mm) fixed below the cursor rail. The results obtained are graphically represented in Fig. 17.

It is noteworthy that as one of the actuators used an encoder with 500 pulses per revolution, it obtained a lower resolution than the others. The resolution presented a considerable variance in all cases which is connected with the mechanical and electronic limitations of the prototype. However, it was possible to observe that the resolutions remain close to each other in actuators with 600-pulse encoders, and within the expected value according to the mathematical model obtained in Section 3. With an estimated value for the resolution, it was also possible to estimate the maximum linear velocity reached by the modules, equal to approximately 1.29 m/s.

Therefore, based on the results obtained in the experiments, it can be concluded that the structure is valid for the practical tests foreseen with healthy patients.

7.3. Pilot study

Experimental trials have been approved by the ethics committee on human research at the Federal University of Uberlândia (CAAE 01305318.2.0000.5152). The tests were made using the proposed novel BWS in combination with the developed serious game and a treadmill. All participants gave their informed consent before enrollment. The trial was carried out on two healthy volunteers over 18 years of age, one male and the other female. The proposed objectives for the trial are as follows: check the operation of the structure together with the treadmill in operation, with the human gait running; check the control of the position of the main character of the game, during the execution of the human gait; evaluate gameplay and difficulty during actual use; and identify electrical and/or mechanical failures during operation. Two test sessions lasting about 5 min were performed. A photograph of one test session is shown in Fig. 18.

The neutral position of the platform was adjusted according to the height of each participant. Then, the participants were accommodated on the structure, and the treadmill was turned on. Participants walked



Figure 18. Test session with the healthy participant.

on the treadmill for a few minutes without the game running to check if the speed was adequate, and the platform was comfortable. After confirming the initial conditions with the participants, the game was started and the test session was video-recorded. At the end of the session, the recordings were interrupted and the volunteers presented their main impressions of the structure and the serious game.

The first feedback presented by the participants was about the execution of the gait on the treadmill with the platform. Both participants reported being able to walk normally, with little or no influence of the saddle on the movements performed. During the game, participants reported little difficulties in properly moving the character just moving to the left or right of the treadmill. The main causes of this problem were the limited space for lateral displacement. As for the gameplay of the game, the participants contributed to the correction of the position of some obstacles and the bonus cube. In the game event of platform inclination, the participants reported that the displacement was noticeable, being necessary to adjust the gait movements to the imposed position. The video footage of the experimental tests and the computational simulations presented in this paper can be accessed in: <https://drive.google.com/drive/folders/17bZKsnUAPb1jSSVaHco1ahpjLiTBqhZM?usp=sharing>

8. Conclusion

This article has reported the design and operation of a novel active BWS device for gait rehabilitation as the main contribution. The proposed device is a parallel structure with a low level of coupling in the movements, and the analysis of singularities demonstrated a workspace without singular positions. In this way, the structure can be controlled more simply and with actuators more independent of each other, despite the closed-chain configuration, and the optimization of dimensions was not restricted in terms of singular positions. Furthermore, the device was developed to be low cost with the objective of use in low-income countries.

Attention is addressed to its control architecture and its integration in a specifically developed serious game software, which is the objective of stimulating patient interactions. The actuators of the structure

were controlled after applying an optimization by differential evolution to obtain the best control parameters for each actuator. In this way, it was possible to compensate for the nonlinearities and unforeseen factors during the actuator modules' construction process and control the motors. In addition, an assist-as-needed function was applied to enable the patient's motor action without the interference of the equipment when not necessary.

The experimental tests were carried out in the novel active BWS device, integrated into the developed game. The experimental tests demonstrated some constructive aspects to be improved in the structure to offer a better experience during the training sessions. Based on tests carried out with healthy volunteers, it was possible to obtain recommendations for improvements to the main character's control system, assembly of the physical structure, assembly of actuators, and adjustments in the serious game.

For the control of the structure, it is recommended to use, in future works, machine learning to obtain and evaluate the trajectory profile of the healthy human gait in the telemetry of the structure and to control the dead zone of the AAN as a function of deviations observed in this profile. Also, a suggestion for future work is the use of a haptic virtual environment. The next step is to realize clinical tests with poststroke patients.

Accordingly, the proposed device has been submitted for patenting, and it can be further investigated as a tool to assist professionals in procedures of gait rehabilitation.

Author contributions. The authors contributed equally for the preparation of the paper.

Financial support. This work was supported in part by CNPq under Grant 03511/2021-4, CAPES (Finance code 001), and FAPEMIG under Grant APQ-02829-17.

Conflicts of interest. The authors declare no conflicts of interest exist.

Ethical approval. Experimental trials have been approved by the ethics committee on human research at the Federal University of Uberlândia (CAAE 01305318.2.0000.5152).

References

- [1] S. S. Virani, A. Alonso, H. J. Aparicio, E. J. Benjamin, M. S. Bittencourt, C. W. Callaway, A. P. Carson, A. M. Chamberlain, S. Cheng, F. N. Delling, M. S. V. Elkind, K. R. Evenson, J. F. Ferguson, D. K. Gupta, S. S. Khan, B. M. Kissela, K. L. Knutson, C. D. Lee, T. T. Lewis, J. Liu, M. S. Loop, P. L. Lutsey, J. Ma, J. Mackey, S. S. Martin, D. B. Matchar, M. E. Mussolino, S. D. Navaneethan, A. M. Perak, G. A. Roth, Z. Samad, G. M. Satou, E. B. Schroeder, S. H. Shah, C. M. Shay, A. Stokes, L. B. VanWagner, N.-Y. Wang and C. W. Tsao, "Heart disease and stroke statistics – 2021 update," *Circulation* **143**(8), e254–e743 (2021). doi: [10.1161/CIR.0000000000000950](https://doi.org/10.1161/CIR.0000000000000950).
- [2] E. Salvadori, G. Papi, G. Insalata, V. Rinnoci, I. Donnini, M. Martini, C. Falsini, B. Hakiki, A. Romoli, C. Barbato, P. Polcaro, F. Casamorata, C. Macchi, F. Cecchi and A. Poggese, "Comparison between ischemic and hemorrhagic strokes in functional outcome at discharge from an intensive rehabilitation hospital," *Diagnostics* **11**(1), 38 (2021). doi: [10.3390/diagnostics11010038](https://doi.org/10.3390/diagnostics11010038).
- [3] V. L. Felgin, B. Norrving and G. A. Mensah, "Global burden of stroke," *Circ Res V.* **120**(3), 439–448 (2017). doi: [10.1161/CIRCRESAHA.116.308413](https://doi.org/10.1161/CIRCRESAHA.116.308413).
- [4] R. S. Gonçalves and L. A. O. Rodrigues, "Development of nonmotorized mechanisms for lower limb rehabilitation," *Robotica* **40**(1), 1–18 (2021). doi: [10.1017/S0263574721000412](https://doi.org/10.1017/S0263574721000412).
- [5] P.G.G.A. Lobo, V. B. Zanon, D. Lara, V. B. Freire, C. A. Nozawa, J. V. B. Andrade, W. C. Barros and I. G. A. Lobo, "Epidemiology of the ischemic cerebrovascular accident in Brazil in the year of 2019, an analysis from an age group perspective," *Braz. J. Health Rev.* **4**(1), 3498–3505 (2021).
- [6] S. Frenkel-Toledo, S. Ofir-Geva, L. Mansano, O. Granot and N. Soroker, "Stroke lesion impact on lower limb function," *Front. Hum. Neurosci.* **15**, 1–11 (2021). doi: [10.3389/fnhum.2021.592975](https://doi.org/10.3389/fnhum.2021.592975).
- [7] S. Paolucci, M. Iosa, P. Coiro, V. Venturiero, A. Savo, D. De Angelis and G. Morone, "Post-stroke depression increases disability more than 15% in ischemic stroke survivors: A case-control study," *Front. Neurol.* **10**, 926 (2019). doi: [10.3389/fneur.2019.00926](https://doi.org/10.3389/fneur.2019.00926).
- [8] T. Alves, R. S. Gonçalves and G. Carbone, "Serious games strategies with cable-driven robots for bimanual rehabilitation: A randomized controlled trial with Post-Stroke patients," *Front. Robot. AI* **9**, 739088 (2022). doi: [10.3389/frobt.2022.739088](https://doi.org/10.3389/frobt.2022.739088).
- [9] A. M. Barbosa, J. C. M. Carvalho and R. S. Gonçalves, "Cable-driven lower limb rehabilitation robot," *J. Braz. Soc. Mech. Sci.* **40**, 245 (2018).

- [10] B. Hobbs and P. Artemiadis, "A review of robot-assisted lower-limb stroke therapy: Unexplored paths and future directions in gait rehabilitation," *Front. Neurobot.* **14**, 19 (2020). doi: [10.3389/fnbot.2020.00019](https://doi.org/10.3389/fnbot.2020.00019).
- [11] P. Domínguez-Téllez, J. A. Moral-Muñoz, A. Salazar, E. Casado-Fernández and D. Lucena-Antón, "Game-Based virtual reality interventions to improve upper limb motor function and quality of life after stroke: Systematic review and meta-analysis," *Games Health J.* **9**(1, suppl 3), 1–10 (2020).
- [12] H. Kooij, "Design and evaluation of the LOPES exoskeleton robot for interactive gait rehabilitation," *IEEE Trans. Neur. Syst. Rehabil.* **15**(1), 379–386 (2007). doi: [10.1109/TNSRE.2007.903919](https://doi.org/10.1109/TNSRE.2007.903919).
- [13] M. Roberts, *A robot for gait rehabilitation*, Thesis, MIT, 2004, Retrieved from <http://dspace.mit.edu/handle/1721.1/34562>.
- [14] M. Pietrusinski, I. Cajigas, Y. Mizikacioglu, M. Goldsmith, P. Bonato and C. Mavroidis, "Gait Rehabilitation Therapy using Robot Generated Force Fields Applied at the Pelvis," *In: 2010 IEEE Haptics Symposium, HAPTICS* (2010) pp. 401–407. doi: [10.1109/HAPTIC.2010.5444624](https://doi.org/10.1109/HAPTIC.2010.5444624).
- [15] D. Aoyagi, W. E. Ichinose, D. J. Reinkensmeyer and J. Bobrow, "Human Step Rehabilitation Using a Robot Attached To the Pelvis, 2004," *In: ASME International Mechanical Engineering Congress and Exposition*, (2004) p.7.
- [16] T. Aurich-Schuler, A. Gut and R. Labruyère, "The FreeD module for the lokomat facilitates a physiological movement pattern in healthy people – a proof of concept study," *J. NeuroEng. Rehabil.* **16**(1), 26 (2019). doi: [10.1186/s12984-019-0496-x](https://doi.org/10.1186/s12984-019-0496-x).
- [17] M. K. MacLean and D. P. Ferris, "Design and validation of a low-cost bodyweight support system for overground walking," *ASME. J. Med. Dev.* **14**(4), 045001 (2020). doi: [10.1115/1.4047996](https://doi.org/10.1115/1.4047996).
- [18] E. Swinnen, J. P. Baeyens, K. Knaepen, M. Michielsen, R. Clijsen, D. Beckwée and E. Kerckhofs, "Robot-assisted walking with the Lokomat: The influence of different levels of guidance force on thorax and pelvis kinematics," *Clin. Biomech.* **30**(3), 254–259 (2015).
- [19] S. Hesse, H. Schmidt, C. Werner and A. Bardeleben, "Upper and Lower Extremity Robotic Devices for Rehabilitation and for Studying Motor Control," *In: Current Opinion in Neurology* (Lippincott Williams Wilkins, 2003).
- [20] B. W. Liang, W. H. Wu, O. G. Meijer, J. H. Lin, G. R. Lv, X. C. Lin, M. R. Prins, H. Hu, J. H. van Dieen and S. M. Bruijn, "Pelvic step: The contribution of horizontal pelvis rotation to step length in young healthy adults walking on a treadmill," *Gait Posture* **39**(1), 105–110 (2014).
- [21] A. I. Kapandji, *The Physiology of The Joints*, vol. 3 (Churchill Livingstone, London, 1974).
- [22] C. L. Lewis, N. M. Laudicina, A. Khoo and K. L. Loverro, "The human pelvis: Variation in structure and function during gait," *Anat. Rec. (Hoboken)*, **300**(4), 633–642 (2017). doi: [10.1002/ar.23552](https://doi.org/10.1002/ar.23552). PMID: 28297184; PMCID: PMC5545133.
- [23] T. Ohnuma, G. Lee and N.Y. Chong, "Development of JARoW-II active robotic walker reflecting pelvic movements while walking," *Intel. Serv. Robot.* **10**(2), 95–107 (2017). doi: [10.1007/s11370-016-0212-7](https://doi.org/10.1007/s11370-016-0212-7).
- [24] J. F. Veneman, J. Menger, E. H. F. van Asseldonk, F. C. T. van der Helm and H. van der Kooij, "Fixating the pelvis in the horizontal plane affects gait characteristics," *Gait Posture* **28**(1), 157–163 (2008).
- [25] C. Gosselin, T. Laliberté and A. Veillette, "Singularity-Free kinematically redundant planar parallel mechanisms with unlimited rotational capability," *IEEE Trans. Robot.* **31**(2), 457–467 (2015).
- [26] C. M. Gosselin, M. T. Masouleh, V. Duchaine, P.-L. Richard, S. Foucault and X. Kong, "Parallel Mechanisms of the Multipteron Family: Kinematic Architectures and Benchmarking," *In: Proceedings 2007 IEEE International Conference on Robotics and Automation* (2007), pp. 555–560. doi: [10.1109/ROBOT.2007.363045](https://doi.org/10.1109/ROBOT.2007.363045).
- [27] J. M. Selig, *Geometrical Foundations of Robotics* (World Scientific, 2000). 152 p. ISBN-10: 9810241135. doi: [10.1142/4257](https://doi.org/10.1142/4257)
- [28] R. S. Gonçalves and H. I. Krebs, "MIT-Skywalker: Considerations on the design of a body weight support system," *J. Neuroeng. Rehabil.* **14**, 88, 11 pages (2017) doi: [10.1186/s12984-017-0302-6](https://doi.org/10.1186/s12984-017-0302-6).
- [29] J. J. Uicker, G. R. Penneck, J. E. Shigley and J. M. McCarthy, "Theory of Machines and Mechanisms," *In: Journal of Mechanical Design* (Oxford Press, 2003).
- [30] M. R. Haghjoo, H. Lee, M. R. Afzal, A. Eizad and J. Yoon, "Mech-walker: A novel single-DOF linkage device with movable frame for gait rehabilitation," *IEEE/ASME Trans. Mechatron.* **26**(1), 13–23 (2021) doi: [10.1109/TMECH.2020.2993799](https://doi.org/10.1109/TMECH.2020.2993799).
- [31] R. S. Gonçalves, T. Hamilton, A. D. Ali, H. Hiroaki and H. I. Krebs, "MIT-Skywalker: Evaluating Comfort of Bicycle/Saddle Seat," *In: 2017 International Conference on Rehabilitation Robotics (ICORR)* (2017), pp. 516–520. doi: [10.1109/ICORR.2017.8009300](https://doi.org/10.1109/ICORR.2017.8009300).
- [32] M. Fadali and A. Vizioli, *Digital Control Engineering: Analysis and Design* (Elsevier Science, 2009).
- [33] R. S. Gonçalves, J. C. M. Carvalho and F. S. Lobato, "Design of a robotic device actuated by cables for human lower limb rehabilitation using self-adaptive differential evolution and robust optimization," *Biosci. J.*, 1689–1702 (2016). doi: [10.14393/BJ-v32n1a2016-32436](https://doi.org/10.14393/BJ-v32n1a2016-32436).
- [34] H. J. Asl, T. Narikiyo and M. Kawanishi, "An assist-as-needed control scheme for robot-assisted rehabilitation," *2017 American Control Conference (ACC)*, 2017, pp. 198–203, doi: [10.23919/ACC.2017.7962953](https://doi.org/10.23919/ACC.2017.7962953).
- [35] L. A. O. Rodrigues, L. A. Gaspar and R. S. Gonçalves, "Serious Games Integrated With Rehabilitation Structures and Assist-as-Need Techniques," *In: Handbook of Research on Promoting Economic and Social Development Through Serious Games*, (O. Bernardes and V. Amorim, eds.), vol. 1, 1st edn. (IGI Global, 2022) pp. 1–665.
- [36] R. S. Gonçalves and L. A. O. Rodrigues, "Development of a Novel Parallel Structure for Gait Rehabilitation," *In: Advances in Computational Intelligence and Robotics*, vol. 1, 1st edn. (IGI Global, 2020) pp. 42–81.